

On the population III binary black hole mergers beyond the pair-instability mass gap

Kotaro Hijikawa,^{1*} Ataru Tanikawa,² Tomoya Kinugawa,³ Takashi Yoshida^{4,1} and Hideyuki Umeda¹

¹*Department of Astronomy, Graduate School of Science, The University of Tokyo, 7-3-1 Hongo, Bunkyo-ku, 113-0033 Tokyo, Japan*

²*Department of Earth Science and Astronomy, College of Arts and Sciences, The University of Tokyo, Meguro-ku, Tokyo, Japan*

³*Institute for Cosmic Ray Research, The University of Tokyo, Kashiwa, Chiba, Japan*

⁴*Yukawa Institute for Theoretical Physics, Kyoto University, Kitashirakawa Oiwakecho, Sakyo-ku, Kyoto 606-8502, Japan*

Accepted XXX. Received YYY; in original form ZZZ

ABSTRACT

We perform a binary population synthesis calculation incorporating very massive population (Pop.) III stars up to $1500 M_{\odot}$, and investigate the nature of binary black hole (BBH) mergers. Above the pair-instability mass gap, we find that the typical primary black hole (BH) mass is $135\text{--}340 M_{\odot}$. The maximum primary BH mass is as massive as $686 M_{\odot}$. The BBHs with both of their components above the mass gap have low effective inspiral spin ~ 0 . So far, no conclusive BBH merger beyond the mass gap has been detected, and the upper limit on the merger rate density is obtained. If the initial mass function (IMF) of Pop. III stars is simply expressed as $\xi_m(m) \propto m^{-\alpha}$ (single power law), we find that $\alpha \gtrsim 2.8$ is needed in order for the merger rate density not to exceed the upper limit. In the future, the gravitational wave detectors such as Einstein telescope and Pre-DECIGO will observe BBH mergers at high redshift. We suggest that we may be able to impose a stringent limit on the Pop. III IMF by comparing the merger rate density obtained from future observations with that derived theoretically.

Key words: stars: Population III, binaries: general, black hole mergers, gravitational waves

1 INTRODUCTION

The gravitational wave (GW) observations have been conducted by the GW observatories, the advanced laser interferometer gravitational wave observatory (aLIGO) and advanced VIRGO, and the new GW catalog, GWTC-2, was recently released by the LIGO Scientific Collaboration and the Virgo Collaboration (Abbott et al. 2020). This catalog includes 50 GW sources and 47 of which are binary black holes (BBHs). The typical mass of the detected BBHs is $\sim 30 M_{\odot}$, and this is heavier than that of X-ray binary BHs.

Origins of BBH mergers have been proposed by many authors: field population (Pop.) I or II binary stars (e.g., Belczynski et al. 2020; Kruckow et al. 2018), dynamical interactions in star clusters (e.g., Rodriguez et al. 2016; Di Carlo et al. 2020; Kumamoto et al. 2020), AGN disks (e.g., Tagawa et al. 2020), and triple or multiple star systems (e.g., Antonini et al. 2017). Pop. III binary stars can also become BBH mergers. The typical mass of Pop. III BBHs is $\sim 30 M_{\odot} + 30 M_{\odot}$ (e.g. Kinugawa et al. 2014, 2020), and this is consistent with the observation (Kinugawa et al. 2021). Therefore, Pop. III binary stars are one of the promising origins of BBH mergers.

Previously, Belczynski et al. (2004), Kinugawa et al. (2014, 2020) and Tanikawa et al. (2021) performed binary population synthesis calculations for Pop. III stars and predicted the property of BBH mergers. The maximum zero-age main-sequence (ZAMS) masses in their calculations are $500 M_{\odot}$, $150 M_{\odot}$ and $300 M_{\odot}$, respectively. According to Pop. III star formation simulations (e.g., Susa et al. 2014; Hirano et al. 2015), there is a chance that Pop. III stars as

massive as $\sim 1000 M_{\odot}$ could be formed (e.g., Hirano et al. 2015), although the typical mass is $10\text{--}100 M_{\odot}$. Future GW observatories, such as Cosmic Explorer (Reitze et al. 2019), Einstein telescope (Punturo et al. 2010; Sathyaprakash et al. 2012) and Pre-DECIGO (Kawamura et al. 2006; Nakamura et al. 2016) can detect very massive compact binary mergers (total mass $\sim 100\text{--}1000 M_{\odot}$) up to the redshift $z \sim 10\text{--}1000$. If there are BBHs originating from very massive Pop. III stars, these observatories may be able to detect them. Therefore, in this Letter, we focus on the very massive Pop. III stars up to $1500 M_{\odot}$ and investigate the contribution of very massive Pop. III stars to the BBH merger by means of binary population synthesis in preparation for future observations.

2 METHOD

2.1 Binary Population Synthesis

In order to perform a population synthesis calculation, we use the binary population synthesis code (Tanikawa et al. 2021), which is an upgraded version of BSE (Hurley et al. 2000, 2002)¹. In our code, the fitting formulae for extremely metal poor stars were implemented (Tanikawa et al. 2020, 2021). We use the same mass transfer rate for the stable Roche-lobe overflow and tidal coefficient factor E as in Kinugawa et al. (2020).

We use the $\alpha\lambda$ formalism for common envelope evolution (Webbink 1984) and set $\alpha_{\text{CE}} = 1$ and $\lambda_{\text{CE}} = 1$. We adopt the ‘rapid’

* E-mail: hijikawa@astron.s.u-tokyo.ac.jp

¹ <http://astronomy.swin.edu.au/~jhurley/>

model in [Fryer et al. \(2012\)](#) with the modification for the pulsational pair-instability and pair-instability supernova (see equations 5–7 in [Tanikawa et al. 2021](#)). We assume that the mass of a BH formed through pulsational pair-instability is $45 M_{\odot}$, and the minimum helium core mass of direct collapse is $135 M_{\odot}$ in the same way as [Belczynski et al. \(2016\)](#).

2.2 Initial Conditions

In this study, we follow the evolution of 10^6 binaries consisting of ZAMS stars with the metallicity $Z = 10^{-8} Z_{\odot}$. Although we adopt the metallicity $Z = 10^{-8} Z_{\odot}$ for Pop. III stars ($Z = 0$), this difference has little effect on our results for the following reason. As the abundance of heavy elements in a $Z = 10^{-8} Z_{\odot}$ star is extremely low, the CNO cycle does not operate initially. The abundance of carbon, nitrogen and oxygen are increased by the triple alpha reaction, and then the CNO cycle commences. These evolutionary properties are the same as those of $Z = 0$ stars. Therefore, the difference in metallicity, $Z = 0$ and $Z = 10^{-8} Z_{\odot}$, has little effect on the stellar evolution.

We use the following initial distributions for the primary mass, mass ratio, and orbital separation. The initial primary mass $m_{\text{ZAMS,p}}$ distribution is logarithmically flat ($\xi_m(m_{\text{ZAMS,p}}) \propto m_{\text{ZAMS,p}}^{-1}$), and the mass range is $10\text{--}1500 M_{\odot}$. The initial mass ratio q distribution is flat ($\xi_q(q) \propto \text{const.}$), and the range is $q_{\text{min}}\text{--}1$, where $q_{\text{min}} = 10M_{\odot}/m_{\text{ZAMS,p}}$. The initial orbital separation a distribution is logarithmically flat, and the range is $a_{\text{min}}\text{--}10^5 R_{\odot}$, where a_{min} is determined so that the ZAMS radius does not exceed the Roche lobe radius. In this study, we assume that the initial eccentricity is zero.

We adopt the star formation history in [de Souza et al. \(2011\)](#) for Pop. III stars, but reduce it by a factor of three ([Inayoshi et al. 2016](#); [Kinugawa et al. 2020](#)). We assume that the binary fraction f_b is 0.5.

3 RESULTS

3.1 Mass Distribution

The mass distribution of BBHs which merge within a Hubble time is shown in [Figure 1](#). The distribution is divided into three sub-populations due to the pair-instability mass gap. Hereafter, we call the combination of low mass BH ($\lesssim 50 M_{\odot}$) and low mass BH ‘low mass + low mass’, that of low mass BH and high mass BH ($\gtrsim 130 M_{\odot}$) ‘low mass + high mass’, and that of high mass BH and high mass BH ‘high mass + high mass’.

The peak of high mass primary BH is around $140\text{--}180 M_{\odot}$. The BBH with the most massive primary BH in our calculation is the pair of $686 M_{\odot}$ BH and $219 M_{\odot}$ BH, and their ZAMS masses are $1220 M_{\odot}$ and $360 M_{\odot}$, respectively. We show in [Figure 2](#) the evolutionary channel leading to this BBH. This BBH is formed through double common envelope scenario in which both of the stars are giant phases with a clear core–envelope structure. The primary ZAMS stars having a ZAMS mass higher than $\sim 1220 M_{\odot}$ cannot contribute to the BBH merger. The reason for this is as follows. A massive Pop. III star with a ZAMS mass higher than $\sim 600 M_{\odot}$ extremely expands, can reach the Hayashi track during the main sequence (MS) phase, and has a convective envelope when it is still in its MS phase. Therefore, if such a massive Pop. III MS star fills its Roche lobe, the mass transfer may become unstable, and the binary system enters a common envelope phase. After that, the binary system always coalesces because the MS star does not have a clear entropy jump between its core and envelope, and it will no longer evolve to a BBH. In order to avoid this

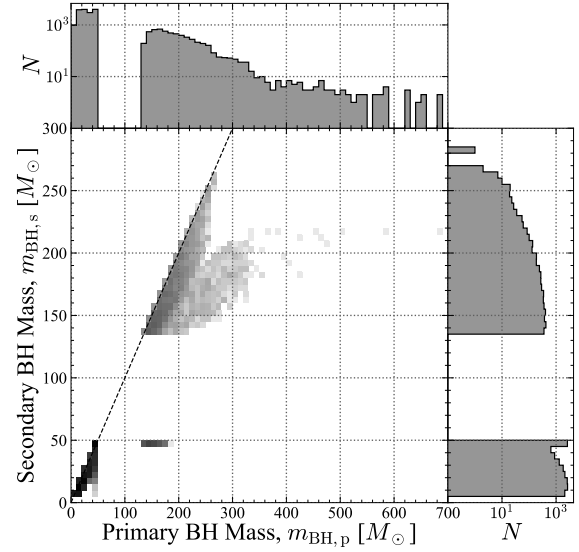


Figure 1. Mass distribution of the BBHs which merge within a Hubble time. The dashed black line indicates the line where primary mass $m_{\text{BH,p}}$ is equal to the secondary mass $m_{\text{BH,s}}$. Each 1D histogram and the shades of color for 2D histogram are on a log-scale.

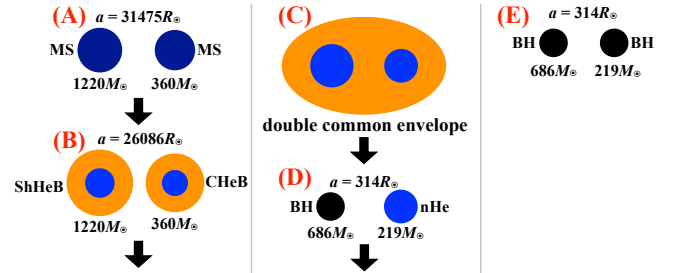


Figure 2. Evolutionary channel leading to the BBH with the most massive primary BH. ‘CHeB’, ‘ShHeB’ and ‘nHe’ stand for the core helium burning phase, shell helium burning phase and naked helium star, respectively.

common envelope episode, the orbital separation needs to be large enough not to fill the Roche lobe during the MS phase.

Hereafter, in order to understand why there is an upper limit on the primary ZAMS mass of merging BBHs, we consider the dependence of the merging timescale of the binary system on the primary ZAMS mass. The merging timescale through GW emission is expressed as $t_{\text{GW}} \propto a^4 m_{\text{BH,p}}^{-2}$, where a is the orbital separation. Based on the above discussion, $a \propto r_{\text{giant,p}}$, where $r_{\text{giant,p}}$ is the primary radius in the giant phase. $r_{\text{giant,p}} \propto m_{\text{ZAMS,p}}^{0.6}$ for Pop. III stars with $m_{\text{ZAMS,p}} \gtrsim 600 M_{\odot}$, and $m_{\text{BH,p}} \propto m_{\text{ZAMS,p}}$. Therefore, $t_{\text{GW}} \propto m_{\text{ZAMS,p}}^{0.4}$. As the primary ZAMS mass increases, the merging timescale increases, and exceeds a Hubble time at a critical ZAMS mass. That is why there is an upper limit on the primary ZAMS mass of merging BBHs. If we use a smaller (larger) $\alpha_{\text{CE}} \lambda_{\text{CE}}$, the maximum mass of merging BBHs is expected to get larger (smaller), because how much the orbital separation shrinks due to the common envelope friction depends on $\alpha_{\text{CE}} \lambda_{\text{CE}}$.

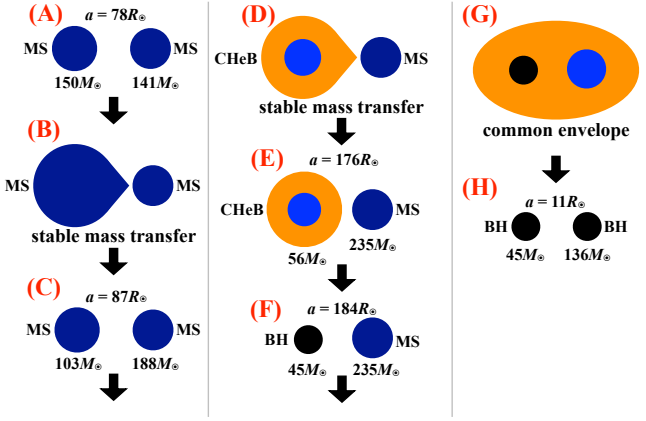


Figure 3. An example evolutionary channel leading to ‘low mass + high mass’.

As can be seen from Figure 1, the number of the primary BH mass decreases sharply at $\sim 340 M_{\odot}$, which is equal to the helium core mass of a $600 M_{\odot}$ Pop. III ZAMS star. This reason is as follows. In our calculation, all ‘high mass + high mass’ BBHs are formed through double common envelope phase, and some of them undergo a stable mass transfer before the double common envelope phase. As mentioned earlier, a Pop. III star with the ZAMS mass $\geq 600 M_{\odot}$ becomes a red supergiant when it is still in its MS phase. Therefore, if the primary ZAMS mass is $\geq 600 M_{\odot}$, the mass transfer may become unstable, and thus the binary systems coalesce, because the primary star does not have a clear entropy jump between its core and envelope. The binary systems can not form BBHs.

In our calculation, all ‘low mass + high mass’ BBHs have $\sim 45 M_{\odot}$ secondary BHs, and those BHs are formed through pulsational pair-instability. An example evolutionary path to ‘low mass + high mass’ is shown in Figure 3. The primary ZAMS mass is $\sim 150 M_{\odot}$, and it will generally cause a pair-instability supernova without mass loss through mass transfer. However, the mass transfer rate is so high that the primary star significantly loses its mass to the secondary star, and can avoid a pair-instability supernova.

3.2 Spin Distribution

In Figure 4, we show the effective inspiral spin parameter χ_{eff} distribution. Since we do not assume the kick, no negative χ_{eff} is obtained.

In our calculation, all ‘high mass + high mass’ BBHs are formed through double common envelope phase. If a binary system enters a double common envelope phase, both stars lose their hydrogen envelopes and spin angular momenta. Therefore, both dimensionless spins of ‘high mass + high mass’ are very low, and 99.8 % of ‘high mass + high mass’ BBHs have χ_{eff} less than 0.1.

On the other hand, χ_{eff} of ‘low mass + high mass’ peaks at around 0.75–0.80. Since the secondary BH progenitor of ‘low mass + high mass’ significantly loses its mass to the primary BH progenitor due to stable mass transfer (the phase B and D in Figure 3), the secondary spin $\chi_{\text{BH},s}$ of all ‘low mass + high mass’ is about 0. Thanks to the short orbital separation after the common envelope phase, the primary BH progenitor can be highly spun up by tidal interaction. Therefore, $\chi_{\text{BH},p}$ peaks at around 1, even though the primary BH progenitor loses its hydrogen envelope and angular momenta during the common envelope phase. When the primary spin is 1, secondary spin is 0, secondary mass is $45 M_{\odot}$, and both spin vectors are aligned

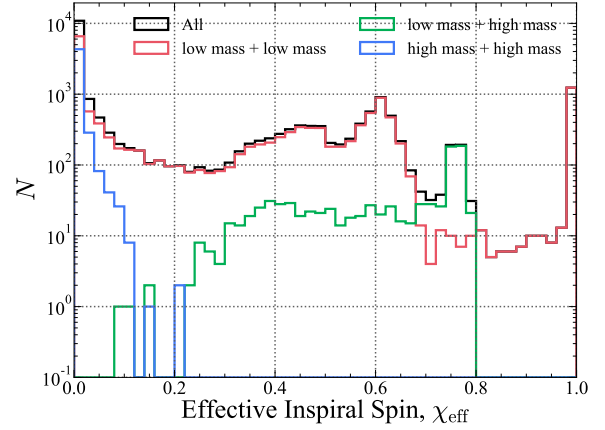


Figure 4. Effective inspiral spin parameter distribution of the BBHs which merge within a Hubble time. The black solid line indicates the effective inspiral spin distribution of all the BBHs. The red, green, and blue lines correspond to the ‘low mass + low mass’, ‘low mass + high mass’, and ‘high mass + high mass’, respectively.

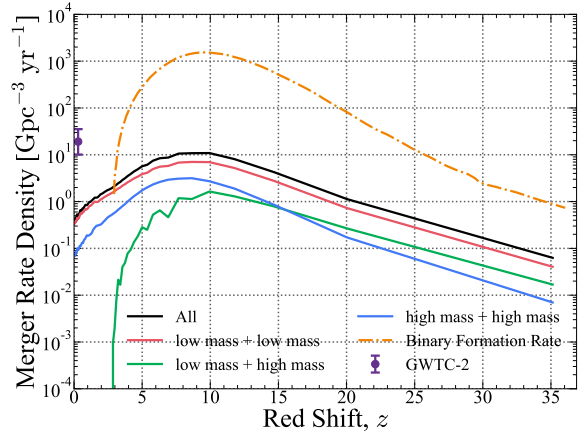


Figure 5. Redshift evolution of merger rate density when the IMF is $\xi_m(m_{\text{ZAMS},p}) \propto m_{\text{ZAMS},p}^{-1}$. The color codes are the same as Figure 4. The purple circle with the error bar indicates the merger rate density estimated from GW observation (The LIGO Scientific Collaboration et al. 2020) in the current universe. The orange dash-dot curve indicates the redshift evolution of the binary formation rate density in number, based on de Souza et al. (2011).

with the orbital angular momentum vector,

$$\chi_{\text{eff}} = \frac{m_{\text{BH},p}\chi_{\text{BH},p} + m_{\text{BH},s}\chi_{\text{BH},s}}{m_{\text{BH},p} + m_{\text{BH},s}} = \frac{m_{\text{BH},p}}{m_{\text{BH},p} + 45}. \quad (1)$$

Since the primary BH mass of ‘low mass + high mass’ is 135–180 M_{\odot} , $\chi_{\text{eff}} = 0.75$ –0.80. Therefore, χ_{eff} of ‘low mass + high mass’ peaks at around 0.75–0.80.

3.3 Merger Rate Density

The merger rate density evolution is shown in Figure 5. In the current universe ($z = 0$), the merger rate density of all Pop. III BBHs and

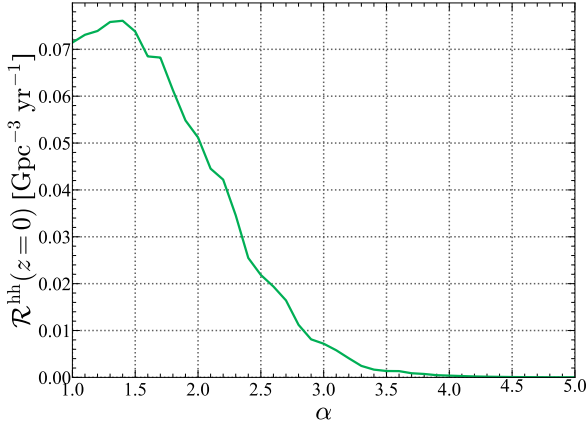


Figure 6. Dependence of $\mathcal{R}^{\text{hh}}(z=0)$ on the exponent of IMF α .

‘high mass + high mass’ BBHs are $\mathcal{R}^{\text{all}}(z=0) = 0.383 \text{ Gpc}^{-3} \text{ yr}^{-1}$ and $\mathcal{R}^{\text{hh}}(z=0) = 0.0714 \text{ Gpc}^{-3} \text{ yr}^{-1}$, respectively. The delay time of ‘low mass + high mass’ is so short that the merger rate density $\mathcal{R}^{\text{hh}}(z)$ is 0 where $z \lesssim 3$.

Our merger rate density of BBHs beyond the mass gap is higher than the upper limit obtained from GW observations. We discuss this disagreement in the next section.

4 DISCUSSION

So far, no BBH merger beyond the pair-instability mass gap has been observed (but see [Fishbach & Holz 2020](#); [Nitz & Capano 2021](#)). According to [María Ezquiaga & Holz \(2020\)](#), the current GW detectors can observe the BBH mergers beyond the mass gap if they exist within their detection horizons. In the absence of detections, they also set the upper limit on the merger rate density above the mass gap at $z=0$ to be $0.01 \text{ Gpc}^{-3} \text{ yr}^{-1}$. Our merger rate density of ‘high mass + high mass’ $\mathcal{R}^{\text{hh}}(z=0)$ is $0.0714 \text{ Gpc}^{-3} \text{ yr}^{-1}$ and is higher than this upper limit. The slope of the Pop. III IMF may be responsible for this discrepancy. Although the Pop. III IMF is not well understood, we adopt the logarithmically flat IMF ($\xi_m(m_{\text{ZAMS,p}}) \propto m_{\text{ZAMS,p}}^{-1}$) in this study. In order to decrease $\mathcal{R}^{\text{hh}}(z=0)$, the Pop. III IMF needs to be steeper or have a cutoff. Here, we investigate how $\mathcal{R}^{\text{hh}}(z=0)$ would change if a different IMF is adopted. We simply assume that the Pop. III IMF is expressed as a single power law, i.e., $\xi_m(m_{\text{ZAMS,p}}) \propto m_{\text{ZAMS,p}}^{-\alpha}$. Figure 6 shows the dependence of $\mathcal{R}^{\text{hh}}(z=0)$ on the exponent of IMF α . In order for $\mathcal{R}^{\text{hh}}(z=0)$ not to exceed the upper limit, $0.01 \text{ Gpc}^{-3} \text{ yr}^{-1}$, α must be greater than 2.8. Note that, the Pop. III star formation rate and common envelope parameters we adopt may affect our result. For example, the Pop. III star formation rate is lower, less steeper IMFs (smaller α) are permissible.

We also obtain the redshift evolution of the merger rate density when $\alpha = 2.8$ (Figure 7). The merger rate density of all Pop. III BBHs evolves with redshift according to $(1+z)^{1.21}$ within $z < 2$, and the local merger rate density of all the BBHs $\mathcal{R}^{\text{all}}(z=0)$ is $2.89 \text{ Gpc}^{-3} \text{ yr}^{-1}$. The merger rate density peaks at around $z \sim 8$, and this reflects the peak of star formation rate. [Kinugawa et al. \(2020\)](#) also performed population synthesis calculations and derived that the merger rate density of Pop. III BBH mergers at $z=0$ is $3.34\text{--}21.2 \text{ Gpc}^{-3} \text{ yr}^{-1}$.

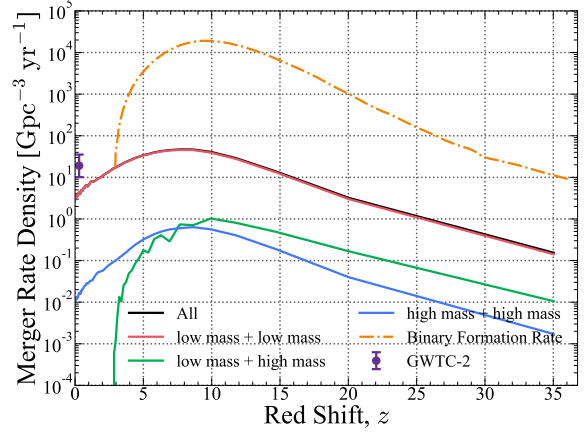


Figure 7. Redshift evolution of merger rate density when $\alpha = 2.8$. The color codes and line styles are the same as Figure 5.

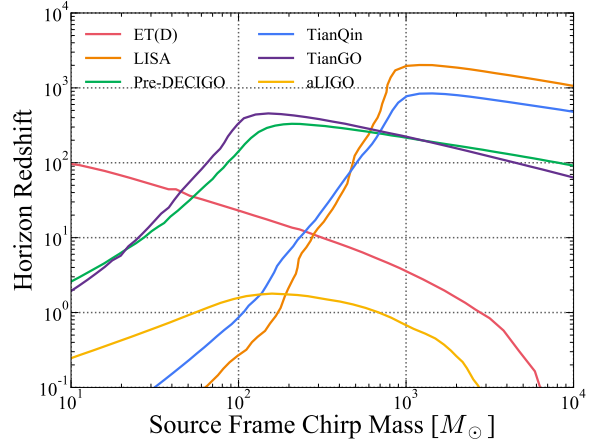


Figure 8. Horizon redshift of GW detectors for face-on compact binary mergers. The red, orange, green, blue, purple and yellow solid lines indicates the horizons of Einstein telescope, LISA, Pre-DECIGO, TianQin, TianGO and aLIGO.

Our merger rate density is roughly consistent with theirs. The BBH merger rate density estimated by [The LIGO Scientific Collaboration et al. \(2020\)](#) from GW observations is $19.1^{+16.2}_{-9.0} \text{ Gpc}^{-3} \text{ yr}^{-1}$ at $z=0$. Thus, some portions of BBHs observed by aLIGO and Virgo may be Pop. III origin.

In the future, the third generation ground-based GW observatories, such as Einstein telescope ([Punturo et al. 2010](#); [Sathyaprakash et al. 2012](#)), and space-borne GW observatories, such as LISA ([Amaro-Seoane et al. 2017](#)), Pre-DECIGO ([Kawamura et al. 2006](#); [Nakamura et al. 2016](#)), TianQin ([Luo et al. 2016](#); [Wang et al. 2019](#)), and TianGO ([Kuns et al. 2020](#)) will operate. The detection horizons of these detectors and aLIGO are shown in Figure 8. Compared to aLIGO, these observatories will detect many compact binary mergers, and will observe BBHs beyond the mass gap up to $z \sim 10\text{--}1000$. Furthermore, by comparing the merger rate density obtained from observation with that derived theoretically, we may be able to impose a stringent limit on the Pop. III IMF. Here, assuming $\alpha = 2.8$, we estimate the detec-

Table 1. Detection rate of Pop.III BBH mergers beyond the mass gap when $\alpha = 2.8$.

Observatory	Detection rate [yr^{-1}]
Einstein telescope	126.1
LISA	1.1
Pre-DECIGO	200.9
TianGO	200.9
TianQin	7.9

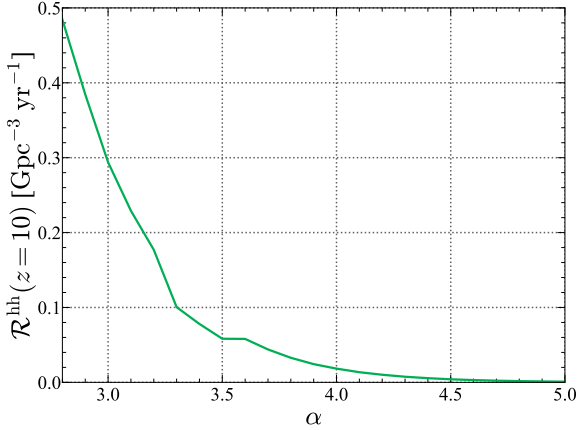


Figure 9. Relation between the merger rate density of BBHs beyond the mass gap at $z = 10$ $\mathcal{R}^{\text{hh}}(z = 10)$ and the exponent of Pop. III IMF α .

tion rate of BBHs beyond the mass gap for some GW detectors, and the results are summarized in Table 1. In our calculation, most of the BBHs beyond the mass gap have the chirp mass of $100\text{--}300 M_{\odot}$. Pre-DECIGO and TianGO can see beyond the beginnings of Pop. III star formation in this mass range, and the detection rate is as high as 200.9 yr^{-1} . The horizon redshift of LISA in this mass range is lower than that of the others, and thus the detection rate is also lower. Since $\alpha \gtrsim 2.8$ is needed as discussed above, the detection rates in Table 1 can also be interpreted as upper limits.

Let us consider that future GW detectors observe BBH mergers, and the merger rate density at $z = 10$ is obtained. We investigate how the exponent α is restricted from the merger rate density of BBHs beyond the mass gap at $z = 10$, $\mathcal{R}^{\text{hh}}(z = 10)$ (see Figure 9). For example, if $\mathcal{R}^{\text{hh}}(z = 10) = 0.1\text{--}0.3 \text{ Gpc}^{-3} \text{ yr}^{-1}$, the exponent of IMF is restricted to 3.0–3.3. In this way, we may be able to impose a stringent restrictions on the Pop. III IMF by future GW observations. Note that we assume that all BBH mergers beyond the mass gap at $z = 10$ are originating from Pop. III stars. In this Letter, we consider only the single power law IMF for Pop. III stars. However, a double power law IMF or an IMF with a cutoff are also possible candidates for the Pop. III IMF. In the future study, we will adopt such an IMF and investigate how we can impose restrictions on Pop. III IMF from GW observations.

5 SUMMARY

In this Letter, we performed a binary population synthesis incorporating very massive Pop. III stars up to $1500 M_{\odot}$ and investigated

the sub-populations beyond the pair-instability mass gap. Our main results are as follows.

The typical primary BH mass of ‘high mass + high mass’ is $135\text{--}340 M_{\odot}$, and the maximum primary BH mass is as high as $686 M_{\odot}$. χ_{eff} of ‘high mass + high mass’ peaks at around 0, and 99.8 % of those have $\chi_{\text{eff}} \lesssim 0.1$. In order for the merger rate density of BBHs beyond the mass gap not to exceed the upper limit (María Ezquiaga & Holz 2020), the exponent α of single power law IMF needs to be greater than 2.8. When $\alpha = 2.8$, space-borne GW observatories, Pre-DECIGO and TianGO, will be able to detect as much as ~ 200 BBHs beyond the mass gap per year. We suggest that we may be able to impose a stringent limit on the Pop. III IMF by comparing the merger rate density obtained from future observations with that derived theoretically.

ACKNOWLEDGEMENTS

This work was supported by JSPS KAKENHI grant No. 17H06360 and 19K03907 (A. T.), 21K13915 (T. K.), 20H05249 (T. Y.), and 17H01130 and 17K05380 (H. U.), and by the University of Tokyo Young Excellent Researcher program (T. K.). We use the Python packages, `numpy` (van der Walt et al. 2011) and `matplotlib` (Hunter 2007) for our analysis.

DATA AVAILABILITY

Results will be shared on reasonable request to authors.

REFERENCES

- Abbott R., et al., 2020, arXiv e-prints, p. [arXiv:2010.14527](https://arxiv.org/abs/2010.14527)
- Amaro-Seoane P., et al., 2017, arXiv e-prints, p. [arXiv:1702.00786](https://arxiv.org/abs/1702.00786)
- Antonini F., Toonen S., Hamers A. S., 2017, *ApJ*, **841**, 77
- Belczynski K., Bulik T., Rudak B., 2004, *ApJ*, **608**, L45
- Belczynski K., et al., 2016, *A&A*, **594**, A97
- Belczynski K., et al., 2020, *A&A*, **636**, A104
- Di Carlo U. N., et al., 2020, *MNRAS*, **498**, 495
- Fishbach M., Holz D. E., 2020, *ApJ*, **904**, L26
- Fryer C. L., Belczynski K., Wiktorowicz G., Dominik M., Kalogera V., Holz D. E., 2012, *ApJ*, **749**, 91
- Hirano S., Hosokawa T., Yoshida N., Omukai K., Yorke H. W., 2015, *MNRAS*, **448**, 568
- Hunter J. D., 2007, *Computing in Science and Engineering*, **9**, 90
- Hurley J. R., Pols O. R., Tout C. A., 2000, *MNRAS*, **315**, 543
- Hurley J. R., Tout C. A., Pols O. R., 2002, *MNRAS*, **329**, 897
- Inayoshi K., Kashiyama K., Visbal E., Haiman Z., 2016, *MNRAS*, **461**, 2722
- Kawamura S., et al., 2006, *Classical and Quantum Gravity*, **23**, S125
- Kinugawa T., Inayoshi K., Hotokezaka K., Nakauchi D., Nakamura T., 2014, *MNRAS*, **442**, 2963
- Kinugawa T., Nakamura T., Nakano H., 2020, *MNRAS*, **498**, 3946
- Kinugawa T., Nakamura T., Nakano H., 2021, *MNRAS*, **504**, L28
- Kruckow M. U., Tauris T. M., Langer N., Kramer M., Izzard R. G., 2018, *MNRAS*, **481**, 1908
- Kumamoto J., Fujii M. S., Tanikawa A., 2020, *MNRAS*, **495**, 4268
- Kuns K. A., Yu H., Chen Y., Adhikari R. X., 2020, *Phys. Rev. D*, **102**, 043001
- Luo J., et al., 2016, *Classical and Quantum Gravity*, **33**, 035010
- María Ezquiaga J., Holz D. E., 2020, arXiv e-prints, p. [arXiv:2006.02211](https://arxiv.org/abs/2006.02211)
- Nakamura T., et al., 2016, *Progress of Theoretical and Experimental Physics*, **2016**, 129301
- Nitz A. H., Capano C. D., 2021, *ApJ*, **907**, L9
- Punturo M., et al., 2010, *Classical and Quantum Gravity*, **27**, 194002
- Reitze D., et al., 2019, in *Bulletin of the American Astronomical Society*, p. 35 ([arXiv:1907.04833](https://arxiv.org/abs/1907.04833))

- Rodriguez C. L., Chatterjee S., Rasio F. A., 2016, [Phys. Rev. D](#), **93**, 084029
- Sathyaprakash B., et al., 2012, [Classical and Quantum Gravity](#), **29**, 124013
- Susa H., Hasegawa K., Tominaga N., 2014, [ApJ](#), **792**, 32
- Tagawa H., Haiman Z., Kocsis B., 2020, [ApJ](#), **898**, 25
- Tanikawa A., Yoshida T., Kinugawa T., Takahashi K., Umeda H., 2020, [MNRAS](#), **495**, 4170
- Tanikawa A., Susa H., Yoshida T., Trani A. A., Kinugawa T., 2021, [ApJ](#), **910**, 30
- The LIGO Scientific Collaboration et al., 2020, arXiv e-prints, p. [arXiv:2010.14533](#)
- Wang H.-T., et al., 2019, [Phys. Rev. D](#), **100**, 043003
- Webbink R. F., 1984, [ApJ](#), **277**, 355
- de Souza R. S., Yoshida N., Ioka K., 2011, [A&A](#), **533**, A32
- van der Walt S., Colbert S. C., Varoquaux G., 2011, [Computing in Science and Engineering](#), **13**, 22

This paper has been typeset from a $\text{\TeX}/\text{\LaTeX}$ file prepared by the author.